TrkA+ Neurons Induce Pathologic Regeneration After Soft Tissue Trauma

Masnsen Cherief, Stefano Negri, Qizhi Qin, Chase A Pagani, Seungyong Lee, Yunzhi Peter Yang, Thomas L Clemens, Benjamin Levi, Aaron W James

Stem Cells Translational Medicine, 2022, **11**, 1165–1176
https://doi.org/10.1093/stcltm/szac073
Advance access publication 12 October 2022
Original Research

TrkA+ Neurons Induce Pathologic Regeneration After Soft Tissue Trauma

Masnsen Cherief[1], Stefano Negri[1,2], Qizhi Qin[1], Chase A. Pagani[5], Seungyong Lee[1], Yunzhi Peter Yang[6], Thomas L. Clemens[3,4], Benjamin Levi[*,5], Aaron W. James[*,1]

[1]Department of Pathology, Johns Hopkins University, Baltimore, MD, USA
[2]Department of Orthopaedics and Traumatology, University of Verona, Verona, Italy
[3]Department of Orthopaedics, Johns Hopkins University, Baltimore, MD, USA
[4]Baltimore Veterans Administration Medical Center, Baltimore, MD, USA
[5]Center for Organogenesis and Trauma, Department of Surgery, University of Texas Southwestern, Dallas, TX, USA
[6]Department of Orthopaedic Surgery, Stanford University, Stanford, CA, USA

[*]Corresponding authors: Aaron W. James, M.D., Ph.D., 720 Rutland Avenue, Room 524A, Baltimore, MD 21205, USA. Tel: +1 410 502 4143; Email: awjames@jhmi.edu; or, Benjamin Levi, M.D., 5323 Harry Hines Blvd. Building E, Room 514A, Dallas, TX, USA. Tel: +1 214 533 7680; Email: Benjamin.Levi@utsouthwestern.edu

Abstract

Heterotopic ossification (HO) is a dynamic, complex pathologic process that often occurs after severe polytrauma trauma, resulting in an abnormal mesenchymal stem cell differentiation leading to ectopic bone growth in soft-tissues including tendons, ligaments, and muscles. The abnormal bone structure and location induce pain and loss of mobility. Recently, we observed that NGF (Nerve growth factor)-responsive TrkA (Tropomyosin receptor kinase A)-expressing nerves invade sites of soft-tissue trauma, and this is a necessary feature for heterotopic bone formation at sites of injury. Here, we assayed the effects of the partial TrkA agonist Gambogic amide (GA) in peritendinous heterotopic bone after extremity trauma. Mice underwent HO induction using the burn/tenotomy model with or without systemic treatment with GA, followed by an examination of the injury site via radiographic imaging, histology, and immunohistochemistry. Single-cell RNA Sequencing confirmed an increase in neurotrophin signaling activity after HO-inducing extremity trauma. Next, TrkA agonism led to injury site hyper-innervation, more brisk expression of cartilage antigens within the injured tendon, and a shift from FGF to TGFβ signaling activity among injury site cells. Nine weeks after injury, this culminated in higher overall levels of heterotopic bone among GA-treated animals. In summary, these studies further link injury site hyper-innervation with increased vascular ingrowth and ultimately heterotopic bone after trauma. In the future, modulation of TrkA signaling may represent a potent means to prevent the trauma-induced heterotopic bone formation and improve tissue regeneration.

Key words: Gambogic amide; heterotopic bone; ectopic bone; mesenchymal stem cells; osteogenesis; endochondral ossification; sensory innervation; NGF; nerve growth factor; TrkA.

Received: 25 May 2022; Accepted: 3 September 2022.

Graphical Abstract

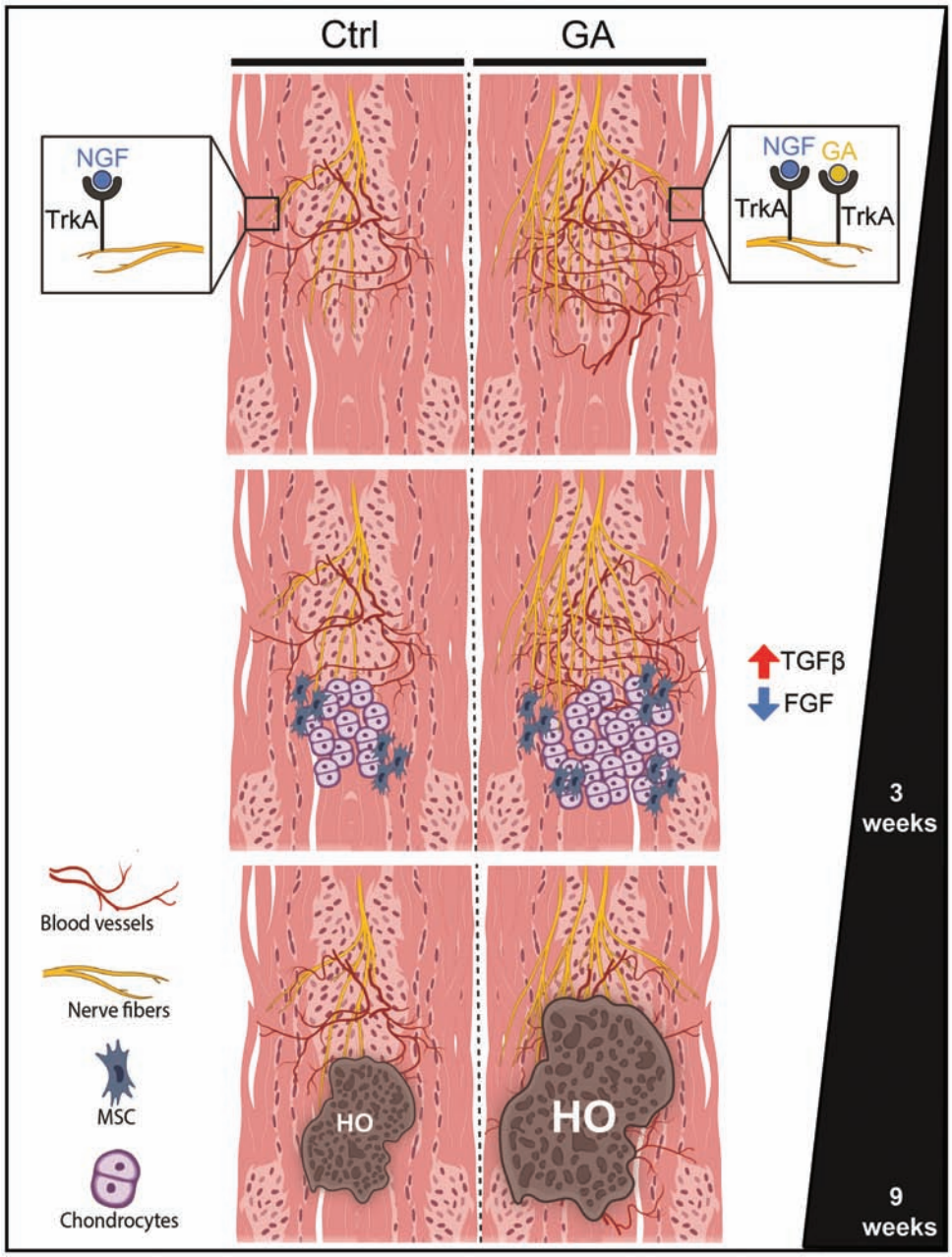

Significance Statement

Heterotopic ossification formation is a common complication of surgery or traumatic injury. Heterotopic ossification represents a major health burden to the patient, associated with pain, mobility impairment, poor wound healing, and increased incidence of disability. Better characterization of the tissues supporting heterotopic ossification is critical to identifying therapies directed against this devastating condition.

Introduction

Heterotopic ossification (HO) is a process of aberrant mesenchymal stem cell differentiation leading to ectopic bone formation often following local trauma and may occur at diverse tissue sites including skeletal muscle, fascia, tendon, and ligament. Following soft-tissue trauma, common features of HO include pain, inflammation, mesenchymal progenitor cell recruitment, chondrogenic differentiation and, finally, ossification.[1] Medical treatment for HO are basically confined to non-steroidal anti-inflammatory medications (NSAIDs) and low-dose radiotherapy.[2,3] Peripheral nerves have been implicated as a potential cellular contribution to HO development in BMP2 (Bone Morphogenetic Protein 2)-induced HO in several preclinical studies.[4-6] Indeed, HO has been described to occur around traumatized nerves.[6,7]

A recent study conducted by our group observed that axonal ingrowth at sites of soft-tissue trauma is a necessary feature for trauma-induced heterotopic bone.[8] In this case, surgical denervation slowed axonal ingrowth, leading to significant delays in cartilage and bone formation at the HO induction site. Likewise, either deletion of (nerve growth factor) or 2 complementary methods to inhibit its receptor TrkA (tropomyosin receptor kinase A) led to similar delays in axonal invasion and osteochondral differentiation. Mechanistically, a combination of single-cell sequencing and immunohistochemistry suggested a shift from TGFβ to FGF signaling activation among pre-chondrogenic cells after surgical denervation. These observations paralleled our earlier work in which TrkA-expressing peripheral afferent nerves were found to be integral cellular components in bone morphogenesis and repair.[9-11] Nevertheless, the extent to which hyper-innervation could drive ectopic bone formation has not been formally assessed.

Here, we sought to enhance the ingrowth of TrkA-expressing nerves during an experimental model of trauma-induced HO.[12,13] Activation of TrkA signaling was achieved by administration of Gambogic amide (GA), a non-peptide small molecule that selectively binds to the juxtamembrane domain of TrkA, inducing TrkA phosphorylation, dimerization, and downstream signaling activation including AKT and MAPK signaling.[14] Unlike NGF itself, GA is not known to produce thermal or mechanical hyperalgesia.[15] Results associate injury site hyper-innervation with heterotopic bone following extremity trauma, and implicate NGF-TrkA signaling as an upstream signaling pathway critical in this process.

Materials and Methods

Animal Use

All animal experiments were carried out in accordance with the Institute for Laboratory Animal Research's Guide for the Use and Care of Laboratory Animals (ILAR, 2011) and were approved by the Johns Hopkins University Institutional Animal Care and Use Committee (IACUC) (MO16M226 & MO19M366). Unless otherwise noted, all animals were housed in IACUC-supervised facilities at 18-22 °C, 12-h light–dark cycle, with ad libitum access to food and water. Jackson Laboratories provided the wild-type C57BL/6J mice (Bar Harbor, ME). All trials were conducted on male 8-week-old mice.

Surgical Procedures

Trauma-induced heterotopic ossification (HO) was produced by complete transection of the Achilles tendon combined with a 30% total body surface area (TBSA) partial thickness burn of the dorsal surface over a 9-week period, as described in our previous findings.[12,13,16] Gambogic amide (GA) was used to activate the TrkA signaling pathway. Animals received 100 µL vehicle control (20% ethanol) or 0.4 mg/kg of GA diluted in 20% ethanol administered by intraperitoneal (IP) injection. Treatment began 24 h prior to burn/tenotomy, and daily thereafter for 2 weeks.

Micro Computed Tomography (MicroCT) Imaging and Analysis

Mouse hind limbs were harvested and imaged 9 weeks post-injury by microCT using a Skyscan 1275 scanner (Bruker-MicroCT, Kontich, Belgium) with the following settings: 65 kV, 153 µA, 1 mm aluminum filter in 180°, 6 frames per 0.3° with a 15-µm voxel size. Images were reconstructed using NRecon. DataViewer software was used to realign the images and quantitative parameters were assessed using Skyscan CTan software (SkyScan, Kontich, Belgium). Scans were analyzed manually by splining around ectopic bone tissue and quantified by CTAn v1.20.

Dual-Energy X-ray Absorptiometry (DXA)

DXA assessment for whole body bone mineral density (BMD) was performed 3 weeks after injury, using a UltraFocus Faxitron equipment (Faxitron Bioptics, Tucson, Arizona). In addition, body weight was recorded on days 1, 7, and 14 after injury.

Serum Alkaline Phosphatase Activity

At 3 weeks post-injury, 200 µL of blood was collected from 3 animals per group. After collection, the blood was allowed to clot by leaving it undisturbed at room temperature for 30 minutes. After 10 minutes of centrifugation at 2000*g*, the supernatant containing the serum was carefully withdrawn. A total of 20 µL of serum was used to measure the alkaline phosphatase activity using a colorimetric assay and following the manufacturer's instructions (ab83369).

Histologic Image Analysis and Histomorphometry

Specimens were harvested and placed in 4% paraformaldehyde (PFA) at 4 °C for 24 h. After sequential washes in PBS × 3, samples were decalcified in 14% EDTA (1:20 volume, Sigma–Aldrich) for 14-28 d at 4 °C. Sagittal sections of the Achilles tendon were obtained using cryosections at 10 or 50 µm thickness. Thin sections (10 µm) were used for all histochemical stains and select immunohistochemistry. The following primary antibodies were used: anti-ACAN (ab3778, 1:200, Abcam), anti-Col2 (ab185430, 1:200, Abcam), anti-ColX (ab58632, 1:200 Abcam), anti-OCN (ab93876, 1:100, Abcam), anti-pSmad2 (44-2446, 1:150, Invitrogen), and anti-pERK1/2 (9101S,1:150, Cell Signaling). Thick sections (50 µm) were used for immunohistochemical stains of blood vessels and nerve fibers. The following primary antibodies were used for thick sections: anti-CD31 (ab28364, 1:200, Abcam), anti-TUBB3 (ab18207, 1:1500, Abcam), and anti-CGRP (C8198, 1:200, Sigma–Aldrich). For cryosections, samples were cryoprotected in 30% sucrose overnight at 4 °C before embedding in OCT (Tissue-Tek 4583, Torrance, CA). Sagittal sections were mounted on adhesive slides (TruBond 380, Matsunami, Bellingham, WA). Histochemical stains included routine Modified Goldner's Trichrome (GMT), and Safranin O/ Fast green (SO/FG). For immunohistochemistry, sections were washed in PBS × 3 for 10 minutes. When 50 µm sections were used, sections were next permeabilized with 0.5% Triton-X for 30 minutes. Next, 10% normal goat serum was applied for 30 minutes, then incubated in primary antibodies overnight at 4 °C in a humidified chamber (Supplementary Table S1). The following day, slides were washed in PBS, incubated in the appropriate secondary antibody, AF594-Goat Anti-Rabbit IgG or Goat Anti-Mouse IgG, for 1 h at 25 °C, then mounted with DAPI mounting solution (Vectashield H-1500, Vector Laboratories, Burlingame, CA). For double-stained immunohistochemistry, first, anti-TUBB3 was incubated overnight a 4 °C, washed 3 times in PBS then incubated with AF594-Goat Anti-Rabbit IgG secondary antibody for 1 h at room temperature. Next, the slides were washed in PBS × 3 for 10 minutes and incubated for 3 h with Alexa Fluor 647 anti-mouse CD31 antibody (102516, 1:50, Biolegend) or with anti-collagen II antibody (MA5-12789,

1:50, Thermofisher). Next, slides were washed in PBS × 3 for 10 minutes then mounted with DAPI mounting solution (Vectashield H-1500, Vector Laboratories, Burlingame, CA) or incubated with AF647-Goat Anti-Mouse IgG for 1 h then washed in PBS × 3 for 10 minutes then mounted with DAPI. Digital images of these sections were captured with 10-100 × objectives using upright fluorescent microscopy (Leica DM6, Leica Microsystems Inc., Buffalo Grove, IL) or confocal microscopy (Zeiss LSM780 FCS, Carl Zeiss Microscopy GmbH, Jena, Germany). Nerve fibers and blood vessels were quantified using volumetric surface renderings using Imaris software v.9.3 (Oxford Instruments, Belfast, UK). For analysis, six 20 × 3-dimensional volumetric regions of interest (2000*400 pixels) were analyzed per sample which were centered around the injured proximal tendon area (Fig. 2 and Supplementary Fig. S3e and S3j, S4c). In addition, longitudinal section slides were stained with Safranin O-Fast Green to assess cartilage area and were stained with modified Goldner's trichrome to evaluate the bone area. The analyses were conducted in the distal Achilles tendon injury site using the OsteoMeasure histomorphometry analysis system (OsteoMetrics, Decatur, GA, USA). Briefly, SO/FG and GMT stained slides were assessed with a microscope with a video camera and displayed in Osteomeasure software. Quantification of staining patterns for the formation of cartilage and bone was performed using manual delineation of tissue edges. The total tissue area of cartilage or bone ROI was manually traced and automated segmentation was used to acquire histomorphometric parameters for ectopic cartilage and bone. Quantification of the pSMAD2/ SMAD2 and pERK1/2/ ERK1/2 staining was performed using a volumetric quantification for nuclear positive staining localized around the Achilles tendon tenotomy site using the Surfaces tool on Imaris 9.3 software.

Western Blot

Three Achilles tendons per group were microdissected from the injury area at 3 wks post-injury. Achilles's tendons were lysed in RIPA buffer (Thermo Fisher Scientific) with a protease inhibitor cocktail (Cell Signaling Technology, Danvers, MA, USA). Protein concentration was determined by BCA assay (Thermo Fisher Scientific). Tissue lysates were separated by SDS-polyacrylamide gel electrophoresis and transferred onto a nitrocellulose membrane. Protein extraction was blocked with 5% bovine serum albumin and incubated with primary antibodies at 4 °C overnight. Finally, membranes were incubated with a horseradish-peroxidase (HRP)-conjugated secondary antibody and detected with ChemiDoc XRS+ System (Bio-rad). Antibodies are listed in Supplementary Table S1.

Single-cell RNA Sequencing Preparation

scRNA sequencing data are publicly available on GEO, GSE150995. Uninjured and post-injured day 7 and 42 harvested tissue samples were processed as previously performed.[17] One mouse, serving as the uninjured control did not undergo the burn/tenotomy surgery. Three to 4 mice underwent the burn/tenotomy injury for each time point. Cells from the uninjured control and the injured mice were harvested 7- and 42-days post-injury. Hind limb tissue was digested in 750 U/mL Typ. 1 Collagenase and 7U/mL Dispase II (Gibco) in Roswell Park Memorial Institute (RPMI) medium at 37 °C under constant agitation at 180 rpm for 45 min. Tissue digestions were quenched in 2% FBS in PBS and filtered through 40 µm sterile strainers. The resulting cells were washed in 2% FBS in PBS, counted and resuspended at a concentration of 1000-1200 cells/µL for viability assays and sequencing. Countess II (Thermo Fisher Scientific) automated counter was used to assess cell viability based on Trypan blue exclusion. Samples with >85% viability were processed for further sequencing. Volumes corresponding to 5000 cell equivalents were removed for processing. RNA libraries were generated from 5000 cells as described below. Library generation was performed using the 10× Genomics Chromium GEM Single Cell 3′ Reagents kit v3.1 following the manufacturer's protocol. Sequencing was performed on the Novaseq 6000 (Illumina, San Diego, CA, USA) S4 flowcell 300 cycle kit, targeting 500M reads/sample (5000 cells, 100K reads/cell), at 300pM (shared flowcells). A read length configuration of 150 × 8 × 150 cycles was used for Read 1, Index, and Read 2, respectively. The University of Michigan Biomedical Core Facilities DNA Sequencing Core used Cell Ranger Single Cell Software Suite 1.3 to execute sample de-multiplexing, barcode processing, and single cell-gene counting (Alignment, Barcoding, and UMI Count).

Bioinformatics Analysis of Single-cell Sequencing Data

Seurat 3.1.1[18] was used for downstream analysis. Cells with total expressed genes in the range of [500, 5000], [500, 6000], or [500, 7500], depending on the replicate, were retained. Cells with a fraction of mitochondrial gene UMIs higher than 0.25 were removed. Filtered replicates were processed as Seurat objects. Two thousand highly variable genes were determined using Seurat's FindVariableFeatures function with default parameters. Replicates were integrated according to the standard Seurat 3 workflow. Counts were normalized and variable genes were calculated (vst method) on every single replicate. To find integration anchors and integrate the replicates, the first 50 dimensions were used. The integrated set was then scaled, regressing out cell cycle gene scores and the fraction of the mitochondrial gene UMIs. Unsupervised clustering led to 25 clusters (Louvain algorithm, resolution 0.35). The code to generate the Seurat object is available at https://github.com/smarini/Single-Cell-Downstream-analysis-Pagani-et-al.-2020. Seurat FindMarkers function using the negative binomial generalized linear model was used to calculate marker genes for each cluster. Genes were ranked according to the difference in the fractions of cells expressing each marker within the cluster versus the rest of the considered cells. Clusters were labeled as cell types according to characteristic genes.

Statistical analysis

Statistical analyses were performed in IBM SPSS Statistics 16.0. Quantitative data are expressed at mean ± SD. A 2-tailed Student's *t* test was used for 2-group comparisons, and a one-way ANOVA test was used for comparisons of 3 or more groups, followed by Tukey's post hoc test. $*P < .05$ and $**P < .01$ were considered significant.

Results

Soft Tissue Trauma Induces Neurotrophin Expression

Extremity trauma was performed to induce heterotopic ossification (HO), as previously described and validated.[12,13] Here, Achilles tenotomy combined with a dorsal burn injury results in HO formation at the injury site via endochondral ossification

over a well characterized 9-week period (Supplementary Fig. S1).[16,17,19] Recently, our group identified that this extremity injury results in an acute increase in NGF (Nerve growth factor) expression at early timepoints, which drives NGF-responsive nerve ingrowth into the incipient HO site.[8] A previously established single-cell RNA sequencing (scRNA-Seq) dataset was used to further interrogate neurotrophins and their receptors after HO inducing injury.[8] Here, local extremity tissues after burn/tenotomy injury were dissociated and analyzed at 7 and 42 days after injury in comparison to uninjured tissues (Fig. 1). Eleven cell clusters were identified including a mesenchymal progenitor cell (MPC), a pericyte, and a Schwann cell cluster (Fig. 1a). Among neurotrophins, *Ngf* and *Bdnf* were most commonly expressed across cell clusters (Fig. 1b). The pericyte cluster showed the highest mean expression for *Ngf* and *Bdnf*, while several the other cell clusters showed lower expression for both *Ngf* and *Bdnf* (also visualized by UMAP projections, Fig. 1c, 1d). In comparison, expression of the neurotrophins *Gdnf* and *Ntf3* showed low expression in this model. Changes in *Ngf* expression across timepoints of HO formation were next visualized by volcano plots (Fig. 1e, 1f). The pericyte cluster showed basal *Ngf* expression before the injury, which was modestly increased during early and later HO formation. Several other populations also showed acute *Ngf* expression after injury only, including Schwann cells and MPC cluster (Fig. 1e).

Neurotrophin receptors were next examined across local cells of the HO site (Supplementary Fig. S2). Low expression of the high-affinity receptor *Ntrk1* was observed across all cell clusters (Supplementary Fig. S2a). Notably, local axons known to express TrkA are not captured in this analysis by virtue of their cell shape. Similar to our prior reports,[8] the low affinity receptor *Ngfr* was expressed in some cell types, and was most notable among the pericyte cluster (Supplementary Fig. S2b, S2c). *Ntrk2* was also expressed among pericyte and MPC clusters before and after injury (Supplementary Fig. S2d, S2e).

TrkA Agonism Increases Nerve Invasion After Extremity Trauma

Next, we investigated the effects of the partial TrkA agonist Gambogic Amide (GA) on innervation after extremity injury. For this purpose, GA was supplied systemically for a 2 week period after injury according to similarly reported treatment regimens in mice.[14,20] The pan-neuronal marker Beta III Tubulin (TUBB3) was used to visualize invading axons within the injured tissues, specifically focusing on sagittal sections of the proximal tenotomy site (Fig. 2b-e). As expected, a qualitative increase in injury site innervation was observed among animals with GA treatment. This difference was most prominent at 3 weeks after injury, in which more frequent TUBB3$^+$ axons were found adjacent to the injured tendon (Fig. 2b, 2c). At 9 weeks, a qualitative increase in nerve fiber frequency was also observed among GA-treated animals (Fig. 2d,e). Quantification of GA-treated tendon injury sites was performed using TUBB3-stained sections (Fig. 2f). Injury sites among GA-treated animals demonstrated a 562.64% and 126.42% increase in TUBB3$^+$ nerve fiber density in relation to control at 3 and 9 weeks, respectively. Similar observations of increased TUBB3$^+$ nerve density were found throughout the injured tissues (Supplementary Fig. S3). To further inquire potential systemic effects of GA, mouse weight, whole-body BMD, and serum alkaline phosphatase were assessed, which showed no significant difference with GA treatment (Supplementary Fig. S4).

In parallel, immunohistochemistry for the neuropeptide CGRP (calcitonin gene-related peptide) was performed (Fig. 2g-2j). Overall, GA treatment resulted in a similar increase in CGRP immunoreactive nerve fibers within the injury site, which was also most conspicuous at 3 weeks post-injury. Quantification of CGRP$^+$ nerve fiber density showed 92.71% increase at 3 weeks and an 11.88% increase at 9 weeks post-injury with GA treatment. Thus, systemic TrkA agonism with

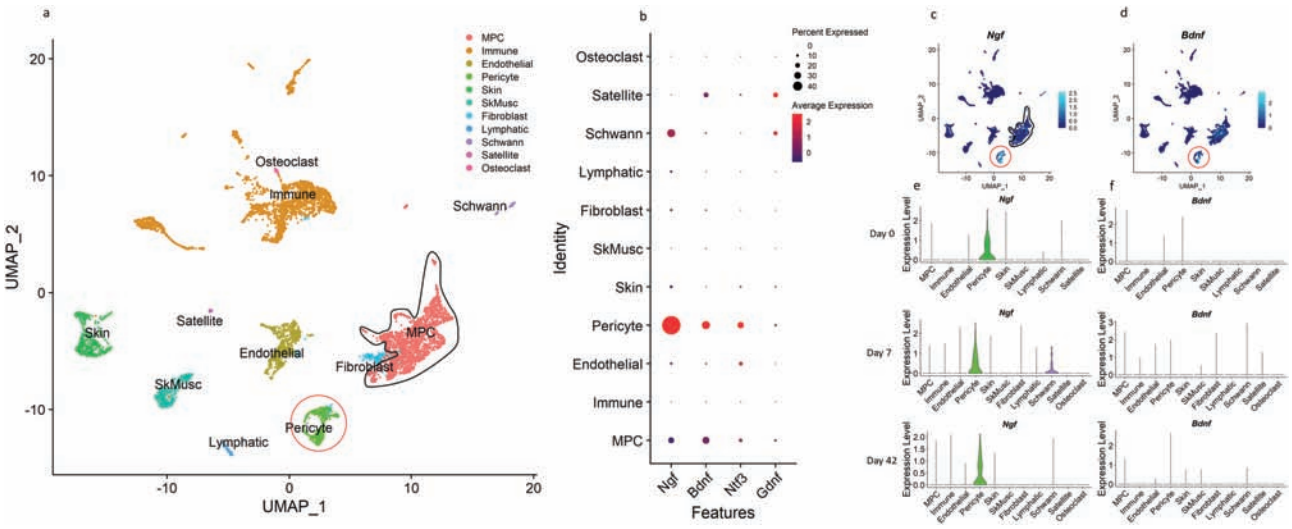

Figure 1. Expression of neurotrophins during the evolution of heterotopic ossification. After HO induction in C57BL/6J mice, the injury site was investigated using single-cell RNA sequencing for up to 42 days. (**a**) UMAP visualization of the 11 cell clusters obtained from the pooled cells across 3-time points (0, 7, and 42 days). Each cell cluster is colored and labeled separately. (**b**) Dot plot visualization of differential gene expression from pooled cells of 3-time points (0, 7, and 42 days) after HO induction. The dot plot shows the relative expression of neurotrophins (*x*-axis) across all cell clusters (*y*-axis). Each dot encodes for both gene detection rate (heat map) and gene average expression (dot diameter). (**c**, **d**) UMAP visualization of (c) *Ngf* and (d) *Bdnf* expression among all the clusters from pooled time points. Red circles indicate pericyte cell clusters. The black surrounded cluster indicates "MPC" cells. (**e**,**f**) Violin plots demonstrating (e) *Ngf* and (f) *Bdnf* expression separately across timepoints. MPC: mesenchymal progenitor cell; SkMusc: skeletal muscle cell. Cells isolated from *N* = 3-4 animals per timepoint.

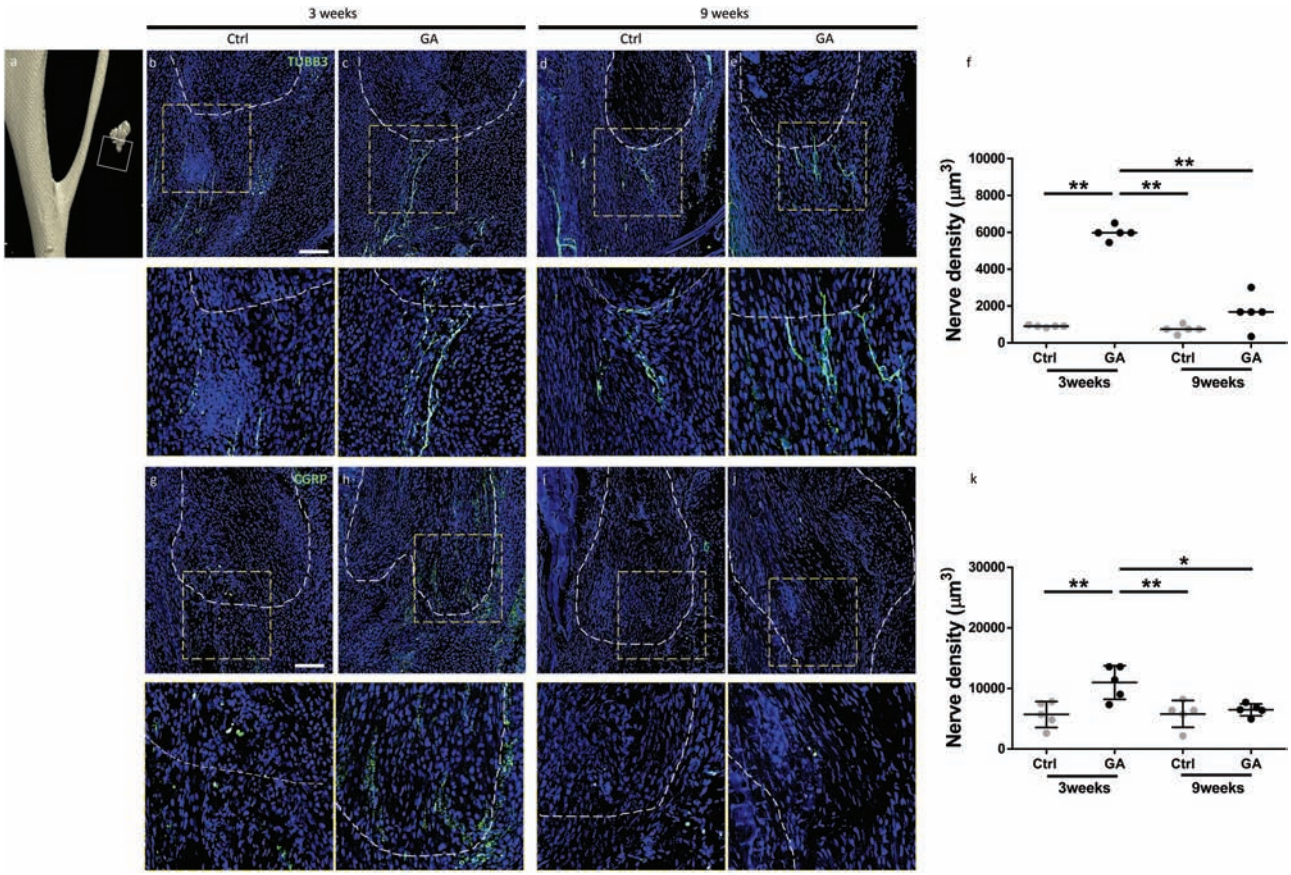

Figure 2. TrkA agonism increases axonal invasion after extremity injury. Analysis was performed on sagittal sections of the proximal tenotomy site, among gambogic amide (GA) and control-treated animals. Analysis performed at 3 and 9 weeks post-injury. (**a**) Representative 3D reconstructions of micro-computed tomography, the white frame shows the proximal HO formation site (**b-e**) Beta III Tubulin (TUBB3) immunohistochemical staining. (**f**) Quantification of TUBB3+ nerve absolute density among GA-treated or control-treated animals. (**g-j**) Calcitonin gene-related peptide (CGRP) immunohistochemical staining. (**k**) Quantification of CGRP+ nerve density among GA treated or control treated animals. Dashed white lines indicate the margins of the Achilles tendon. High magnification images are shown in the yellow dotted frame. Scale bar: 100 µm. For all graphs, each dot represents a single analyzed animal. $N = 5$ animals per group, per timepoint. Statistical analysis was performed using ANOVA with post hoc Tukey's test. $^{*}P < .05$, $^{**}P < .01$.

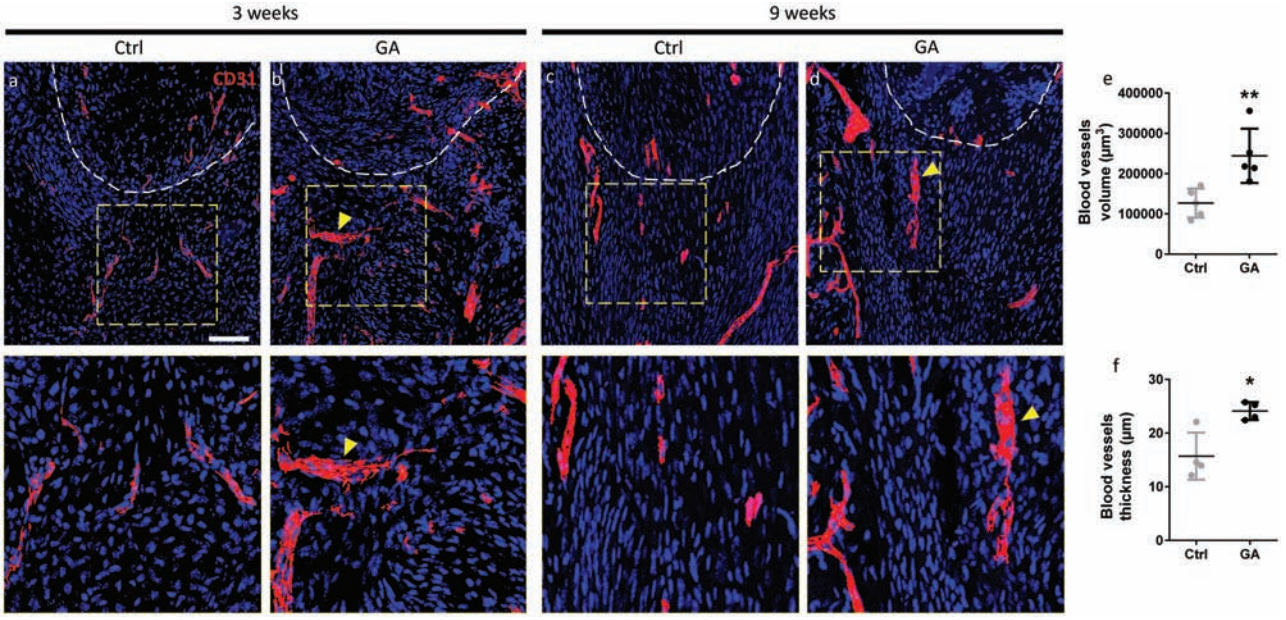

Figure 3. TrkA agonism increases vascularity after extremity injury. Immunohistochemical stains of the vascular endothelial marker CD31, shown within representative sagittal sections of the proximal tenotomy site among Gambogic Amide (GA) and control-treated animals. Images shown at (**a, b**) 3 and (**c, d**) 9 weeks post-injury. (**e**) Quantification of CD31+ blood vessel volume among GA treated or control treated animals at 3 weeks post-injury. (**f**) Quantification of CD31+ blood vessel thickness among GA treated or control treated animals at 3 weeks post-injury. Yellow arrowheads indicate larger caliber blood vessels. Dashed white lines indicate the margins of the Achilles tendon. High magnification images are shown in yellow dotted frame. $N = 5$ animals per group. $^{*}P < .05$, $^{**}P < .01$. Scale bar: 100 µm.

GA increased axonal ingrowth into the soft-tissue injury site, particularly at earlier time points after trauma.

TrkA Agonism Increases Blood Vessel Ingrowth After Trauma

Nerves and blood vessels are well known for influencing one another's growth and trajectory as they sprout to target tissues during organogenesis or repair.[21,22] In our own prior observations during long bone morphogenesis[11] and stress fracture,[10] TrkA inhibition in mice resulted in impaired vascular assembly suggesting strongly in bone tissue that neurovascular ingrowth are functionally linked process. Next, we investigated whether TrkA agonism led to increased vascularization at the site of incipient bone formation. CD31 immunohistochemical staining at the proximal tenotomy site was performed (Fig. 3a-3d). A conspicuous increase in injury site vascularity was observed at 3 weeks among GA-treated animals (Fig. 3a, 3b). This was accompanied by an increase in the thickness of vessels within GA-treated injury sites, suggestive of a quicker maturation of a vascular network (yellow arrowhead, Fig. 3b). A similar observation was made at 9 weeks post-injury (Fig. 3c, 3d), and in particular the number of thicker caliber microvessels was increased with GA treatment (yellow arrowheads). The vascular histomorphometric analysis confirmed a significant increase in both overall blood vessel volume as well as blood vessel thickness among GA-treated samples (Fig. 3e, 3f). The immunohistochemical co-staining of CD31 with TUBB3 shown in Supplementary Fig. S5 displayed a close spatial relationship between nerves and vessels at this time point. Thus, systemic TrkA agonism induces neurovascular ingrowth after extremity trauma.

TrkA Agonism Increases Markers of Endochondral Bone Formation After Trauma

The extent to which increased neurovascular supply at an injury site led to altered expression of chondro-osseous antigens

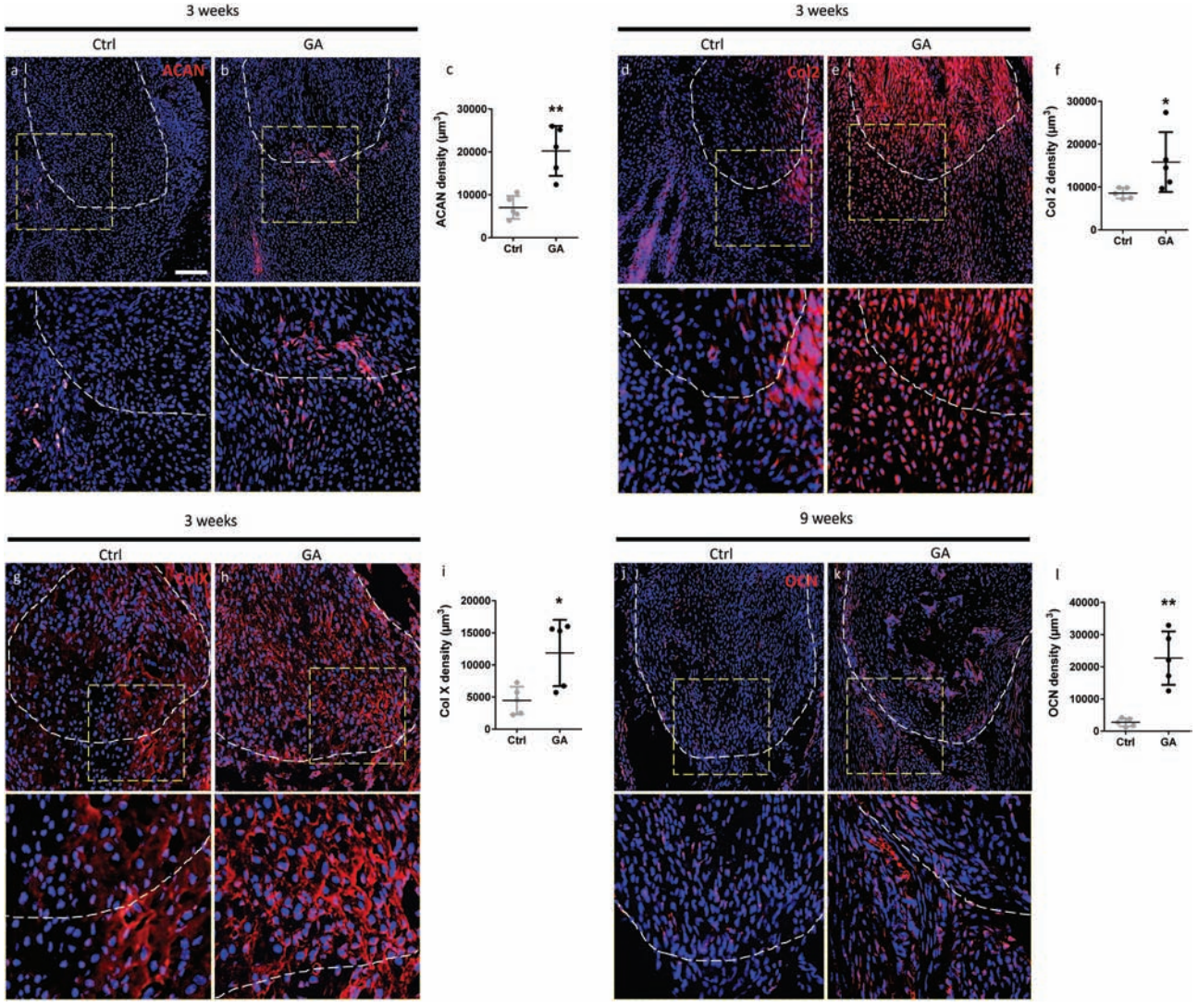

Figure 4. TrkA agonism increases cartilage and bone antigen expression after extremity injury. Immunohistochemical staining within injured tissues of Gambogic Amide (GA) or control treated animals. Representative sagittal sections of the proximal tenotomy site shown, at either 3 or 9 weeks post-injury. (**a, b**) Aggrecan (ACAN) immunohistochemical staining, 3 weeks post-injury. (**c, d**) Type II Collagen (Col2) immunohistochemical staining, 3 weeks post-injury. (**e, f**) Type X Collagen (ColX) immunohistochemical staining, 3 weeks post-injury. (**g, h**) Osteocalcin (OCN) immunohistochemical staining, 9 weeks post-injury. Dashed white lines indicate the margins of the Achilles tendon. High magnification images are shown in yellow dotted frame. $N = 5$ animals per group. $^{*}P < .05$, $^{**}P < .01$. Scale bar: 100 µm.

was next examined (Fig. 4). First, cartilage-associated antigens were assayed by immunohistochemistry at the earlier 3-week timepoint, including Aggrecan (ACAN) (Fig. 4a, 4b), Type II Collagen (Col2) (Fig. 4c, 4d), and Type X Collagen (ColX) (Fig. 4e, 4f). As expected, some immunoreactivity for all cartilage markers was observed across all samples. Further, a conspicuous increase in the distribution and intensity of immunostaining for all markers was observed among the GA treatment group. Next, the terminal osteoblastic marker Osteocalcin (OCN) was assayed at the 9-week timepoint (Fig. 4g, 4h). Similar to prior observations with cartilage markers, systemic TrkA agonism led to an overall increase in OCN immunoreactivity within and around the injured tendon (Fig. 4g, 4h). Co-immunohistochemical staining of TUBB3 and osteochondral antigens further showed a close spatial relationship between nerves and HO formation (Supplementary Figs. S6 and S7). Thus, GA-mediated TrkA agonism results in an increase in markers of endochondral bone formation after trauma.

TrkA Agonism Increases Chondro-Osseous Differentiation After Extremity Trauma

Injury site chondro-osseous differentiation was next assessed by histology and histomorphometry (Fig. 5). Safranin O/Fast Green (SO/FG) was used to highlight glycosaminoglycan accumulation within the cartilaginous phase after tenotomy (Fig. 5a-5d). At 3 weeks, some degree of SO staining was observed across all samples, but a more obvious increase in the degree and expanse of staining was observed among GA-treated animals (Fig. 5a, 5b). At the terminal 9 weeks timepoint, little remaining SO staining was seen across all samples, while fast green counterstaining showed evidence of bone formation within GA-treated sections. Histomorphometric quantification of cartilaginous area at the 3 weeks timepoint showed a relative 148.89% increase among the GA treatment group, at 3 weeks (Fig. 5e). Bone formation after injury was assessed using Goldner's Modified Trichrome (GMT) staining (Fig. 5f-5i). At 3 weeks, no frank bone tissue was yet observed in either treatment group (Fig. 5f, 5g). At 9 weeks post-injury, heterotopic bone with central bone marrow was again observed particularly among GA-treated samples (Fig. 5h, 5i). Histomorphometric quantification of the heterotopic bone area at 9 weeks post-injury showed a 394.62% increase among the GA-treated group (Fig. 5j).

TrkA Agonism Increases Post-Traumatic Heterotopic Bone Formation

Radiographic evidence of bone formation within the injury site was examined (Fig. 6). High-resolution XR imaging at the study endpoint confirmed increased spicules and cloud-like radiodensity within the injury site which were apparent across all samples, but more abundant within GA-treated animals

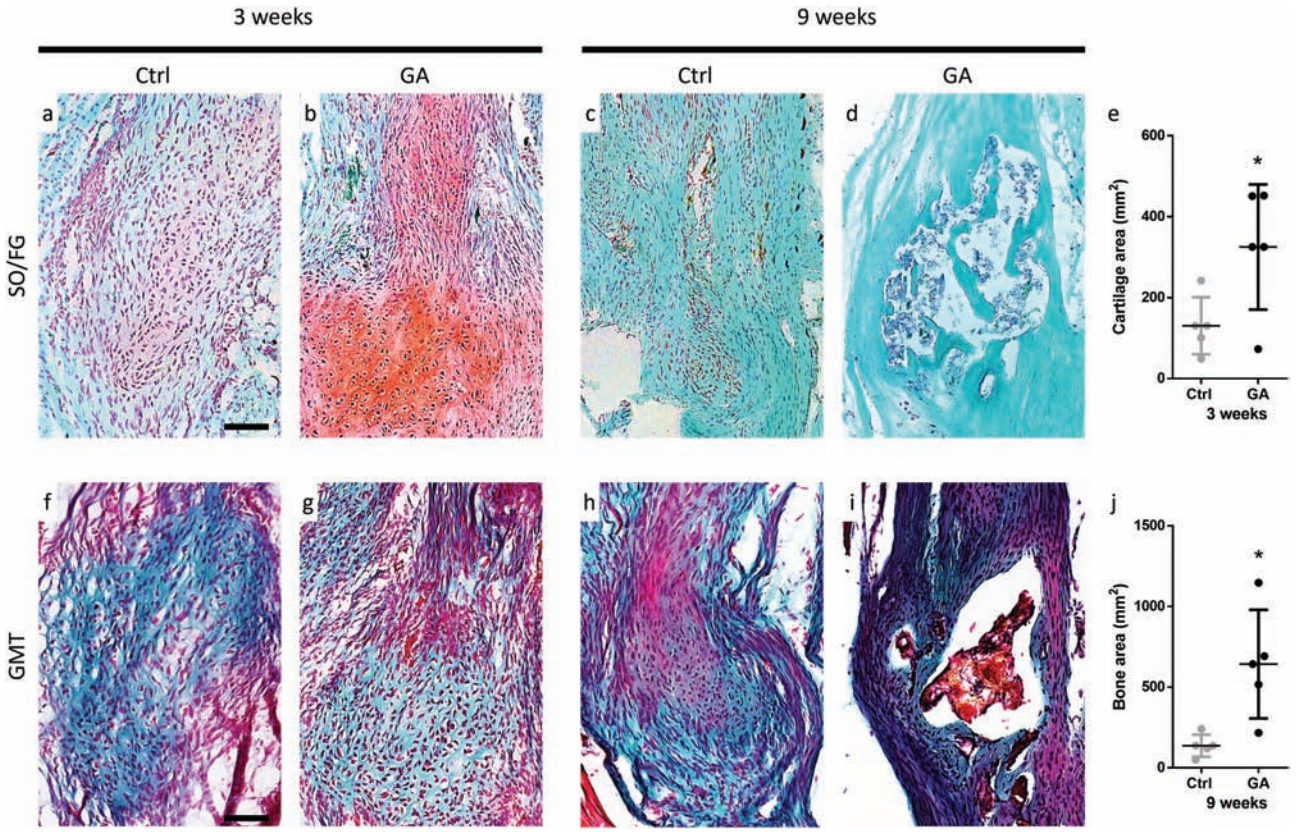

Figure 5. TrkA agonism increases histologic evidence of bone and cartilage accumulation after extremity injury. Histologic assessment of the proximal tenotomy site after induction of heterotopic ossification among Gambogic Amide (GA) or control-treated animals. Assessments performed at 3 and 9 weeks post-injury. (**a-d**) Safranin O/ Fast Green (SO/FG) staining of sagittal cross-sections. Cartilaginous matrix appears orange; counterstain appears green. (**e**) Histomorphometric quantification of cartilaginous area among GA or control-treated animals at 3 weeks post-injury. (**f-i**) Goldner's Modified Trichrome (GMT) staining. (**j**) Histomorphometric quantification of bone area among GA or control-treated animals at 9 weeks post-injury. Scale bar: 100 μm. For all graphs, each dot represents a single analyzed animal. $N = 5$ animals per group. Statistical was analysis performed using a 2-way Student's *t*-test. *$P < .05$.

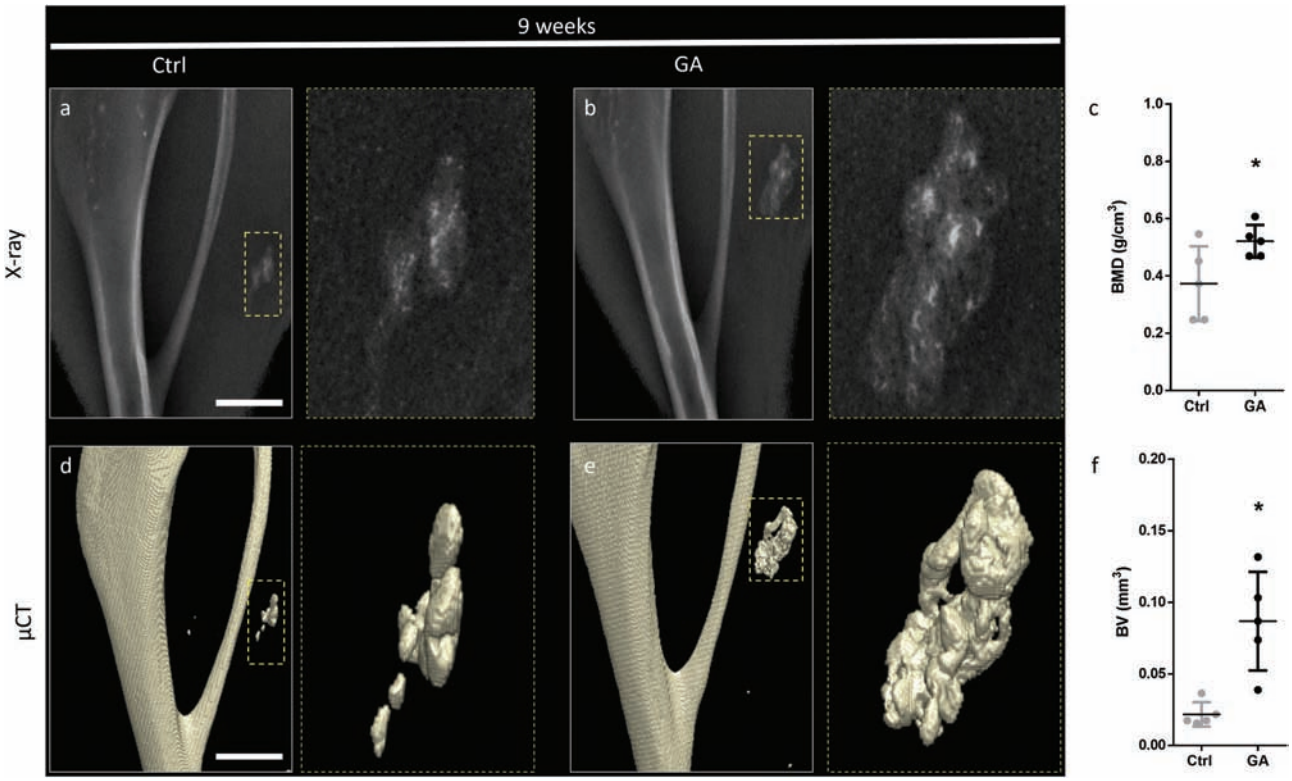

Figure 6. TrkA agonism increases radiographic evidence of heterotopic ossification after extremity injury. (**a,b**) Representative 2D x-ray images of the HO at the proximal tenotomy site among Gambogic Amide (GA) or control-treated animals, shown at 9 weeks post-injury in a medial-to-lateral view. (**c**) Quantification of Bone Mineral Density (BMD) at the injury site by DXA after 9 weeks among GA or control treated animals. (**d,e**) Representative 3D reconstructions of micro-computed tomography (microCT) imaging among Gambogic Amide (GA) or control-treated animals, shown at 9 weeks post-injury in a medial-to-lateral perspective. (**f**) Quantification of Bone Volume (BV) at the injury site after 9 weeks among GA or control-treated animals. High magnification images are shown in yellow dotted frame. Scale bar: 100 μm. For all graphs, each dot represents a single analyzed animal. $N = 5$ animals per group. Statistical analysis was performed using a 2-way Student's *t*-test. $^*P < .05$.

(Fig. 6a,b). Dual XR absorptiometry (DXA) confirmed a significant increase in bone mineral density (BMD) within the injured soft tissue among GA-treated animals (Fig. 6c). μCT imaging was next analyzed, again confirming an increase in heterotopic bone among GA-treated injury sites as visualized using 3D reconstructions (Fig. 6d,e). Quantitative μCT analysis showed a mean 299.91% increase in bone volume within the GA treated group in relation to control (Fig. 6f). Thus, TrkA agonism-associated hyperinnervation is accompanied by an increase in heterotopic formation after trauma.

TrkA Agonism Results in a Shift from FGF to TGFβ Signaling Activation After Trauma

The downstream molecular mechanisms whereby TrkA$^+$ nerve ingrowth enhances aberrant osteochondral differentiation are not yet clear. Previously, surgical denervation in the burn/tenotomy model resulted in a shift from TGFβ to FGF signaling activation among pre-chondrogenic cells (Lee et al., 2020). To extend these findings, immunohistochemical staining for pSmad2 and pERK1/2 was performed to assess activation of TGFβ and FGF signaling pathways, respectively (Fig. 7). At 3 weeks post-injury, pSmad2 demonstrated immunoreactivity across all examined samples, but an overall increase of 245.36% in staining intensity was found among cells within GA-treated samples (Fig. 7a, 7b). Conversely, pERK1/2 immunohistochemical staining demonstrated a 80.56% reduction among injury sites within the GA-treated group (Fig. 7d, 7e). Confirmatory studies to assess changes in TGFβ and FGF signaling activation were performed using Western blotting of the HO induction site (Fig. 7g-7j). Results again showed an overall increase in pSmad2 and reduction in pERK1/2 within the injury site after 3 weeks among GA-treated animals (38.88% increase in pSMAD2/SMAD2 and 33.33% reduction in pERK1/2/ ERK1/2). Thus, TrkA agonism and associated injury site hyper-innervation is associated with a shift in local signaling from FGF to TGFβ activation after trauma.

Discussion

In the present study, we activated TrkA agonism using Gambogic amide to demonstrate the importance of neural infiltration during the soft tissue response to trauma. Using scRNAseq data, we observed an induction of the neurotrophins *Ngf* after trauma. We verified that TrkA agonism indeed results in hyperinnervation of the soft-tissue injury site, and this exuberant ingrowth of nerves is associated with increased vascularity, aberrant endochondral ossification, and an overall shift from FGF to TGFβ signaling activation among cells localized to the injury site.

A common feature of the present and past observations[8] implicate nerve ingrowth after trauma as a regulator of local TGFβ signaling activity. However, the precise source and mechanism of local TGFβ signaling activation within innervated tissues remain unclear. The past analysis supports a peripheral neuronal source of TGFβ ligands.[23,24] Indeed, in our past re-analysis of dorsal root ganglia (DRG) transcriptome,

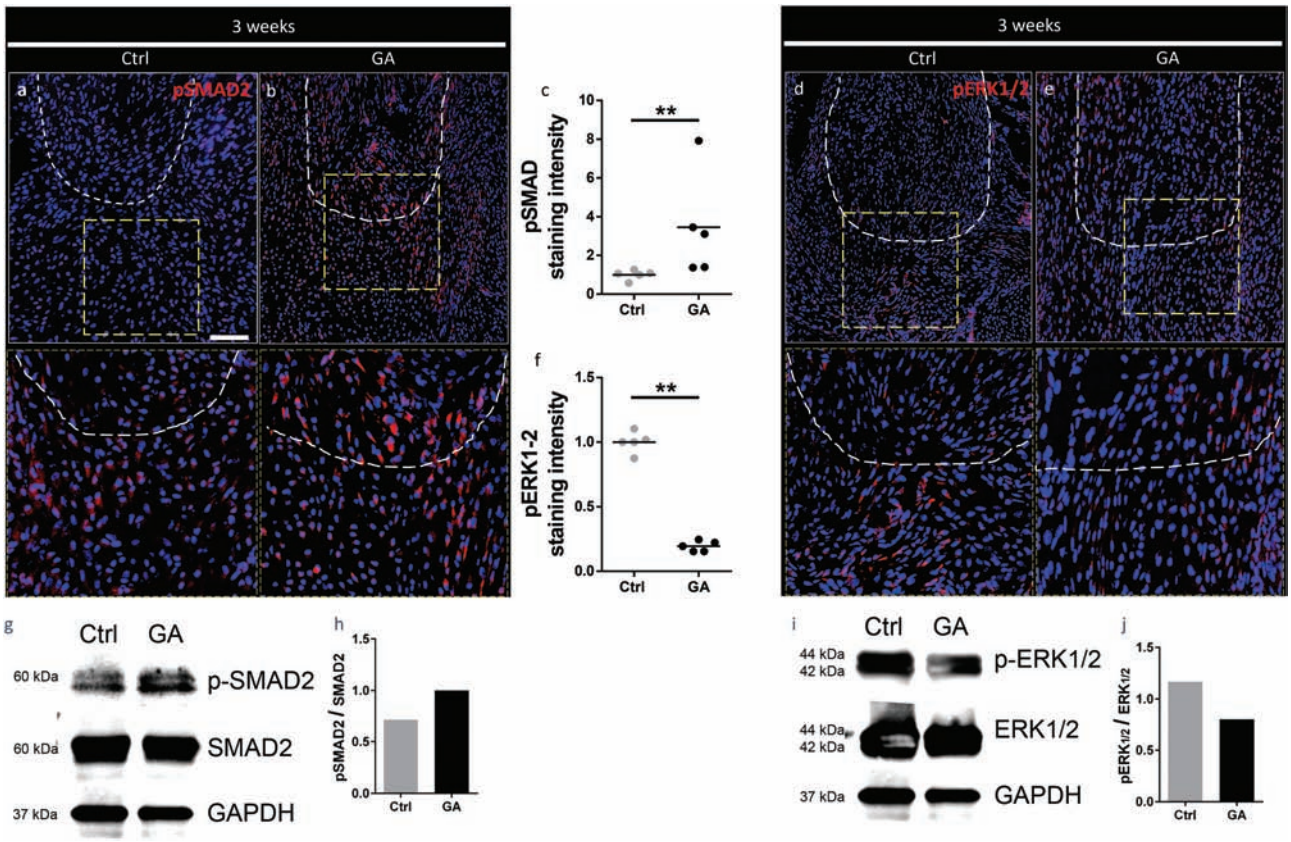

Figure 7. TrkA agonism induces a shift from FGF to TGFβ signaling activation after trauma. (**a-f**) Immunohistochemical stains within representative sagittal sections of the proximal tenotomy site. Sections are taken 3 weeks after injury among Gambogic Amide (GA) and control-treated animals. (**a, b**) Fluorescent immunohistochemistry for pSmad2. (**c**) Quantification of pSmad2+ cells among GA treated or control-treated animals. (**d, e**) Fluorescent immunohistochemistry for pERK1/2. (**f**) Quantification of pERK1/2+ cells among GA treated or control treated. (**g-j**) Western blot analysis of the HO induction site 3weeks after injury. (g) Western blot for pSMAD2, SMAD2 and GAPDH among GA treated or control treated. (h) Quantification of pSMAD2/SMAD2 among GA treated or control treated. (i) Western blot for pERK1/2, ERK1/2 and GAPDH among GA treated or control treated. (i) Quantification of pERK1/2/ERK among GA-treated or control-treated. Dashed white lines indicate the margins of the Achilles tendon. High magnification images are shown in yellow dotted frame. $N = 5$ animals per group. Scale bar: 100 μm. $^{**}P < .01$.

TrkA-expressing nerves express high levels of the TGFβ ligands *Tgfb1*, *Tgfb2*, and *Tgfb3*.[8] Along these lines, recent work performed by our group in the developing mouse skull suggests that TGFβ signaling modifiers may also play a role in axon-to-mesenchymal progenitor cell communication.[25] Contrarily, it is possible that classic neuropeptides derived from sensory axons such as CGRP or Substance P themselves induce local TGFβ expression among other injury-associated cell types, as has been shown in other model systems.[26] For example, the importance of monocyte/macrophage-derived TGFβ1 has been reported in heterotopic bone by our group.[17] Finally, increased TGFβ signaling activity could reflect in general an osteochondrogenic program activation within local mesenchymal cells.

The intersection of nerve and vascular ingrowth at sites of incipient bone formation is another common finding between the present work and past observations within our research groups.[9-11] For example, TrkA inhibition during embryogenesis using a chemical-genetic approach in mice led to a 50% reduction in vascularity of the long bone.[11] In parallel observations, TrkA inhibition during the time period of long bone stress fracture repair led to a similar 18.5%-29.3% reduction in vascularity.[10] The coupling factors for nerve and vessel ingrowth at sites of bone formation have not been elucidated. Certainly, the most obvious candidate neuro-vascular coupling factor is the vascular endothelial growth factor (VEGF). Neural-derived VEGF has been clearly implicated in cutaneous blood vessel patterning,[22,27,28] although the expression of VEGF specifically in skeletal peripheral afferent nerves (PANs) has not yet been established. Alternatively, nerve growth factor (NGF) itself has angiogenic potential and PAN-derived NGF could operate synergistically with VEGF to drive local angiogenesis in the context of heterotopic bone.[29-32]

The interplay between bone and the nervous system is complex. After nervous system injury, bone can be subject to modification ranging from high and aberrant bone-forming activity to the opposite with lower bone formation and increased bone resorption.

The location of injury in the nervous system tends to define the bone-related outcomes. When the injury is in the central nervous system, the blood-brain barrier becomes more permissive and is believed to release osteogenic factors, locally and systemically, participating in the creation of favorable environment for neurogenic heterotopic bone formation.[33] For example, it has been shown that cerebrospinal fluid and serum taken from patients with traumatic brain injury (TBI) contain osteogenic circulating factors, including TGF-β, insulin-like growth factor II, platelet-derived growth factor, interleukin-1, and interleukin-6, that stimulate the differentiation of

mesenchymal cells into osteoblasts.[34] In contrast, when the injury is located in the peripheral nervous system, bone metabolism is altered. It has been observed in rats, that transection of the sciatic nerve reduced femoral bone growth and impaired fracture healing.[35,36] It has also been shown that the destruction of skeletal sensory neurons reduced nerve and bone neuropeptide content, concomitant to a loss of bone mass and strength.[37] The signal transduction pathways by which denervation causes bone loss are unknown. Nonetheless, our recent studies highlighted the significance of peripheral TrkA+ neurons. For the proper development of long bones, NGF-TrkA signaling is essential. NGF promotes the osteoprogenitor lineage progression and vascularization in mouse long bone.[11] In a different work, we showed how NGF-TrkA signaling is crucial for stress fracture repair. Indeed, NGF expression in fracture-associated macrophages and periosteal stromal progenitors enhanced callus ossification and mineralization and were essential for neurovascular sprouting to the fracture.[10] A positive regulatory function of NGF-TrkA signaling during HO development was recently identified by Lee et al. Osteocartilaginous differentiation and HO evolution were attenuated as a result of the pharmacological or genetic suppression of NGF-TrkA signaling. Here we show that activating TrkA signaling led to hyperinnervation that promoted endochondral ossification.[8] These findings collectively suggest injuries to peripheral versus central nervous systems have disparate effects on bone anabolism and HO.

Several important limitations exist in regard to the present results are shown. First, systemic TrkA agonism led to injury site hyperinnervation with a predominant local osteochondral differentiation it is possible that distant sites with altered innervation may have compounded or altered the HO phenotype observed. Second, sympathetic innervation and sympathetic nervous system tone were most likely altered with GA treatment. Sympathetic nerves have been postulated to play a role in HO,[7] and indeed in our past work we observed abnormally high numbers of TH^+ nerve fibers invading the tenotomy site within our model.[8] Future studies must be undertaken which utilize means for either specific sensory or sympathetic nerve ablation, to more precisely define the relative importance of nerve fiber type in driving post-traumatic HO.

In summary, these studies further link injury site hyperinnervation with aberrant stem cell differentiation culminating in heterotopic bone after trauma. In addition, nerve and vascular ingrowth appear to be coupled cellular processes during heterotopic ossification, and likely both are niche factors that predispose to HO after trauma. In the future, inhibition of NGF signaling may represent a potent means to prevent trauma-induced heterotopic bone formation.

Acknowledgments

We thank the JHU microscopy facility for its technical assistance. AWJ is funded by NIH/NIAMS (R01 AR070773, R01 AR068316, R01 AR079171), NIH/NIDCR (R21 DE027922), USAMRAA through the Peer Reviewed Medical Research Program (W81XWH-18-1-0121, W81XWH-18-1-0336), Peer Reviewed Orthopaedic Research Program (W81XWH-20-10795) and Broad Agency Announcement (W81XWH-18-10613), American Cancer Society (Research Scholar Grant, RSG-18-027-01-CSM), and the Maryland Stem Cell Research Foundation. BL is funded by the NIH (NIH1R01AR071379, R01 AR079171) and USAMRAA through the Peer Reviewed Orthopaedic Research Program (W81XWH-20-10795). TLC was supported by the NIH/NIAMS (R01 AR068934), NIH/NIDCR (R21 DE027922), and the VA (Merit Award and Senior Research Career Scientist Award). The content is solely the responsibility of the authors and does not necessarily represent the official views of the National Institute of Health or Department of Defense.

Funding

Research unrelated to the work presented herein was supported in the James Laboratory by Musculoskeletal Transplant Foundation (MTF) Biologics and Novadip Biosciences.

Conflict of Interest

A.W.J.: paid consultant for Novadip and Lifesprout. This arrangement has been reviewed and approved by the Johns Hopkins University in accordance with its conflict of interest policies. All of the other authors declared no potential conflicts of interest.

Author Contributions

M.C.: collection and/or assembly of data, data analysis and interpretation, manuscript writing, final approval of the manuscript. S.N.: collection and/or assembly of data. C.A.P.: data analysis and interpretation. Q.Q.: collection and/or assembly of data, data analysis, and interpretation. S.L.: collection and/or assembly of data. Y.P.Y: data interpretation. T.L.C.: data analysis and interpretation. B.L.: conception and design, data analysis and interpretation. A.W.J.: conception and design, financial support, data analysis and interpretation, manuscript writing, final approval of manuscript.

Data Availability

The data that supports the findings of this study are available in the supplementary material of this article.

Supplementary Material

Supplementary material is available at *Stem Cells Translational Medicine* online.

References

1. Zhang Q, Zhou D, Wang H, Tan J. Heterotopic ossification of tendon and ligament. *J Cell Mol Med*. 2020;24:5428-5437. https://doi.org/10.1111/jcmm.15240
2. Vanden Bossche L, Vanderstraeten G. Heterotopic ossification: a review. *J Rehabil Med*. 2005;37:129-136. https://doi.org/10.1080/16501970510027628
3. Meyers C, Lisiecki J, Miller S, et al. Heterotopic ossification: a comprehensive review. *JBMR Plus*. 2019;3:e10172. https://doi.org/10.1002/jbm4.10172
4. Lazard ZW, Olmsted-Davis EA, Salisbury EA, et al. Osteoblasts have a neural origin in heterotopic ossification. *Clin Orthop Relat Res*. 2015;473:2790-2806. https://doi.org/10.1007/s11999-015-4323-9
5. Olmsted-Davis EA, Salisbury EA, Hoang D, et al. Progenitors in peripheral nerves launch heterotopic ossification. *Stem Cells Transl Med*. 2017;6:1109-1119. https://doi.org/10.1002/sctm.16-0347

6. Salisbury E, Rodenberg E, Sonnet C, et al. Sensory nerve induced inflammation contributes to heterotopic ossification. *J Cell Biochem*. 2011;112:2748-2758. https://doi.org/10.1002/jcb.23225
7. Salisbury E, Sonnet C, Heggeness M, Davis AR, Olmsted-Davis E. Heterotopic ossification has some nerve. *Crit Rev Eukaryot Gene Expr*. 2010;20:313-324. https://doi.org/10.1615/critreveukargeneexpr.v20.i4.30
8. Lee S, Hwang C, Marini S, et al. NGF-TrkA signaling dictates neural ingrowth and aberrant osteochondral differentiation after soft tissue trauma. *Nat Commun*. 2021;12:4939. https://doi.org/10.1038/s41467-021-25143-z
9. Meyers CA, Lee S, Sono T, et al. A Neurotrophic mechanism directs sensory nerve transit in cranial bone. *Cell Rep*. 2020;31:107696.
10. Li Z, Meyers CA, Chang L, et al. Fracture repair requires TrkA signaling by skeletal sensory nerves. *J Clin Invest*. 2019;129:5137-5150.
11. Tomlinson RE, Li Z, Zhang Q, et al. NGF-TrkA signaling by sensory nerves coordinates the vascularization and ossification of developing endochondral bone. *Cell Rep*. 2016;16:2723-2735.
12. Agarwal S, Loder SJ, Sorkin M, et al. Analysis of bone-cartilage-stromal progenitor populations in trauma induced and genetic models of heterotopic ossification. *Stem Cells*. 2016;34:1692-1701.
13. Peterson JR, Agarwal S, Brownley RC, et al. Direct mouse trauma/burn model of heterotopic ossification. *J Vis Exp*. 2015:e52880.
14. Shen J, Yu Q. Gambogic amide selectively upregulates TrkA expression and triggers its activation. *Pharmacol Rep*. 2015;67:217-223.
15. Hsieh YL, Kan HW, Chiang H, et al. Distinct TrkA and Ret modulated negative and positive neuropathic behaviors in a mouse model of resiniferatoxin-induced small fiber neuropathy. *Exp Neurol*. 2018;300:87-99.
16. Agarwal S, Loder S, Cholok D, et al. Surgical excision of heterotopic ossification leads to re-emergence of mesenchymal stem cell populations responsible for recurrence. *Stem Cells Transl Med*. 2017;6:799-806.
17. Sorkin M, Huber AK, Hwang C, et al. Regulation of heterotopic ossification by monocytes in a mouse model of aberrant wound healing. *Nat Commun*. 2020;11:722.
18. Butler A, Hoffman P, Smibert P, et al. Integrating single-cell transcriptomic data across different conditions, technologies, and species. *Nat Biotechnol*. 2018;36:411-420.
19. Hsu GC, Marini S, Negri S, et al. Endogenous CCN family member WISP1 inhibits trauma-induced heterotopic ossification. *JCI Insight*. 2020;5:e135432.
20. Jang SW, Okada M, Sayeed I, et al. Gambogic amide, a selective agonist for TrkA receptor that possesses robust neurotrophic activity, prevents neuronal cell death. *Proc Natl Acad Sci USA*. 2007;104:16329-16334.
21. Martin P, Lewis J. Origins of the neurovascular bundle: interactions between developing nerves and blood vessels in embryonic chick skin. *Int J Dev Biol*. 1989;33:379-387.
22. Li W, Kohara H, Uchida Y, et al. Peripheral nerve-derived CXCL12 and VEGF-A regulate the patterning of arterial vessel branching in developing limb skin. *Dev Cell*. 2013;24:359-371.
23. Rogister B, Delree P, Leprince P, et al. Transforming growth factor beta as a neuronoglial signal during peripheral nervous system response to injury. *J Neurosci Res*. 1993;34:32-43.
24. Rusten TE, Cantera R, Kafatos FC, et al. The role of TGF beta signaling in the formation of the dorsal nervous system is conserved between Drosophila and chordates. *Development*. 2002;129:3575-3584.
25. Tower RJ, Li Z, Cheng YH, et al. Spatial transcriptomics reveals a role for sensory nerves in preserving cranial suture patency through modulation of BMP/TGF-beta signaling. *Proc Natl Acad Sci USA*. 2021;118:e2103087118.
26. Hu D, Chen B, Zhu X, et al. Substance P up-regulates the TGF-beta 1 mRNA expression of human dermal fibroblasts in vitro. *Zhonghua Zheng Xing Wai Ke Za Zhi*. 2002;18:234-236.
27. Mukouyama YS, Shin D, Britsch S, et al. Sensory nerves determine the pattern of arterial differentiation and blood vessel branching in the skin. *Cell*. 2002;109:693-705.
28. Mukouyama YS, Gerber HP, Ferrara N, et al. Peripheral nerve-derived VEGF promotes arterial differentiation via neuropilin 1-mediated positive feedback. *Development*. 2005;132:941-952.
29. Graiani G, Emanueli C, Desortes E, et al. Nerve growth factor promotes reparative angiogenesis and inhibits endothelial apoptosis in cutaneous wounds of Typ. 1 diabetic mice. *Diabetologia*. 2004;47:1047-1054.
30. Lazarovici P, Gazit A, Staniszewska I, et al. Nerve growth factor (NGF) promotes angiogenesis in the quail chorioallantoic membrane. *Endothelium*. 2006;13:51-59.
31. Hansen-Algenstaedt N, Algenstaedt P, Schaefer C, et al. Neural driven angiogenesis by overexpression of nerve growth factor. *Histochem Cell Biol*. 2006;125:637-649.
32. Lazarovici P, Marcinkiewicz C, Lelkes PI. Cross talk between the cardiovascular and nervous systems: neurotrophic effects of vascular endothelial growth factor (VEGF) and angiogenic effects of nerve growth factor (NGF)-implications in drug development. *Curr Pharm Des*. 2006;12:2609-2622.
33. Sullivan MP, Torres SJ, Mehta S, et al. Heterotopic ossification after central nervous system trauma: a current review. *Bone Joint Res*. 2013;2:51-57.
34. Gautschi OP, Toffoli AM, Joesbury KA, et al. Osteoinductive effect of cerebrospinal fluid from brain-injured patients. *J Neurotrauma*. 2007;24:154-162.
35. Madsen JE, Hukkanen M, Aune AK, et al. Fracture healing and callus innervation after peripheral nerve resection in rats. *Clin Orthop Relat Res*. 1998:230-240.
36. Garces GL, Santandreu ME. Longitudinal bone growth after sciatic denervation in rats. *J Bone Joint Surg Br*. 1988;70:315-318.
37. Ding Y, Arai M, Kondo H, et al. Effects of capsaicin-induced sensory denervation on bone metabolism in adult rats. *Bone*. 2010;46:1591-1596.